HD 37017 = V 1046 Ori. A double-lined spectroscopic binary with a B2e He-strong magnetic primary[*]

C.T. Bolton[1][**], **P. Harmanec**[2], **R.W. Lyons**[1,3], **A.P. Odell**[4][***], **and Diane M. Pyper**[5]

[1] David Dunlap Observatory, University of Toronto, P.O. Box 360, Richmond Hill, ON, L4C 4Y6 Canada (bolton@struve.astro.utoronto.ca)
[2] Astronomický ústav Akademie věd České republiky, 251 65 Ondřejov, Czech Republic (hec@sunstel.asu.cas.cz)
[3] Center for Astrophysics and Space Sciences, University of California at San Diego, La Jolla, CA 92093-0424, USA (rlyons@ucsd.edu)
[4] Department of Physics and Astronomy, Northern Arizona University, Flagstaff, AZ 86011, USA (Andy.Odell@nau.edu)
[5] Physics Dept., University of Nevada Las Vegas, Las Vegas, NV 89154, USA (dpsmith@nevada.edu)

Abstract. We report on a detailed spectroscopic and photometric study of V1046 Orionis undertaken to resolve uncertainties about the period(s) and causes of the spectroscopic and photometric variations of this helium-strong star. We have detected the lines of the secondary star in an extensive series of photographic and electronic spectra. This eliminates any doubt about the duplicity of this star. The orbital elements we derive from our measures of these spectra confirm the unusually large orbital eccentricity, $e = 0.433$, for the short, $P = 18{\overset{\text{d}}{.}}65612$, orbital period. The line profiles, V/R ratio of the double Hα emission, residuals of the primary radial velocities from the orbital velocity curve, brightness and colour of the object, magnetic field, and radio emission of this system all vary with a period of $0{\overset{\text{d}}{.}}9011836$. We tentatively follow earlier investigators in interpreting this as the rotational period of the primary and summarize the evidence of the phase shifts among the different phenomena, using the accurate value of the $0{\overset{\text{d}}{.}}9$ period, to put tight constraints on any future model of these changes. We postpone our own attempt at a quantitative modelling of the variations with the $0{\overset{\text{d}}{.}}9$ period for a separate study.

Key words: stars: binaries: spectroscopic – stars: fundamental parameters – stars: oscillations – stars: individual: V 1046 Ori

1. Introduction

V1046 Orionis (HD 37017, HR 1890, BD$-4°$1183, SAO 132317) is a member of the Ori OB1C1 association (Warren and Hesser 1978). Its spectral type has been classified variously

from B1.5V to B2.5IV-V. Walborn (1974) discovered weak Hα emission in the spectrum, which qualifies V 1046 Ori as a Be star according to currently accepted definitions. The presence of variable Hα emission was confirmed by Pedersen (1979). In addition, Leone (1993) reported the presence of weak redshifted emission in the core of Hα on one CCD spectrogram. He interpreted it as evidence for a jet-like outflow of material above the magnetic poles.

Plaskett and Pearce (1931) concluded that V 1046 Ori is a spectroscopic binary based on five spectra obtained between 1924 and 1928. Their conclusion was confirmed by Blaauw and van Albada (1963), who found a period of $18{\overset{\text{d}}{.}}65$ and derived the first orbital elements for the system from measures of 19 spectra obtained at the McDonald Observatory in 1955 and 1956. Recently, Morrell and Levato (1991) measured new radial velocities (hereafter RVs) from 10 Cerro Tololo spectra with a dispersion of either 4.0 or 6.0 nm mm^{-1} (not clearly specified in the paper). They combined their data with the radial velocities of Blaauw and van Albada to improve the orbital period to $18{\overset{\text{d}}{.}}6217$ and calculate new orbital elements.

The similarity between the spectra of V 1046 Ori and HD 37479, the archetype of the helium-strong stars was first noted by Morgan and Lodén (1966). Lester (1972) analyzed line profiles of V 1046 Ori and HR 1891 (HD 37016), a nearby, normal B3V star in the same small cluster in the northern Sword region in Orion, derived from several 0.8 nm mm^{-1} spectra. He found that the He I abundance of V 1046 Ori is about twice that of HD 37016. He concluded there was no evidence of the secondary star in his spectrograms. However, he had to use different $v \sin i$ values for different lines, with values ranging from 95 km s^{-1} for the weak He I λ438.8 nm line to 207 km s^{-1} for He I λ402.6 nm, in order to fit theoretical line profiles based on Klinglesmith's (1971) model atmospheres to the observed profiles!

In January-February 1976, Pedersen and Thomsen (1977) obtained photometry of V 1046 Ori and a number of other helium-peculiar stars with a special set of narrow band filters which allowed them to define an index R that measures strength of the He I λ402.6 nm line. R essentially measures the ratio

I_{line}/I_{cont}; its value thus *decreases* with *increasing* strength of the He I $\lambda402.6$ nm line. They found that the R-index of V 1046 Ori varies with a period of either $9\overset{d}{.}3 \pm 0\overset{d}{.}3$ or $0\overset{d}{.}9015 \pm 0\overset{d}{.}0020$. While they noted that the longer period is approximately one-half of the orbital period, they preferred the shorter period because they expected the helium line strength to vary on the rotational time scale of the star by analogy with the other helium-strong stars.

Groote (1978) combined RVs measured from nine new high-dispersion spectrograms of V 1046 Ori with Blaauw and van Albada's (1963) data and found a period, $0\overset{d}{.}948366$, that satisfied both the RV and R-index data. His RV curve has a single wave, while the R-index curve has a double wave with minima centered on the systemic velocity crossings. Groote (1978) concluded that V 1046 Ori is a short-period spectroscopic binary with a synchronously rotating He-strong primary. However, this model has one surprising feature — an unusually high orbital eccentricity, $e = 0.22$, for such a short orbital period.

Pedersen (1979) obtained additional R-index observations of V 1046 Ori in October and December 1976. When he combined these data with his earlier observations, he was able to improve the value of the period of the R-index variations to $0\overset{d}{.}901175 \pm 0\overset{d}{.}00013$. He found that the R-index variations could also be reconciled with Groote's period, but he preferred the 0.901 day period because the R values have a slightly higher scatter about their phase curve when plotted with the longer period.

Pedersen and Thomsen (1977) obtained $uvby$ photometry of V 1046 Ori at the same time as their R-index observations. These data showed that the light and colours vary with the same period as the R-index. The star is brightest in y and has the smallest c_1 index when the helium lines are strongest. The light variability of V 1046 Ori was discovered independently by Balona (1977), who noted that it was varying slowly in V and U when he used it as one of the comparisons for his observations of 42 Ori. Adelman and Pyper (1985) obtained additional $uvby\beta$ photometry of V 1046 Ori, confirmed the variations with a $0\overset{d}{.}901175$ period and found no evidence of variations in the observed energy distribution of the star other than some changes in the bandpasses affected by strong He I lines. They found variations in $u - b$, but none in $b - y$. They also noted that the Hβ line seems to vary in antiphase with the He I lines.

Groote et al. (1980) obtained infrared $JHKLM$ observations of several helium variables and reported excesses in the M band for most of them, including V 1046 Ori. When their data were published (Groote and Kaufman 1983), it was apparent that they *do not* define a meaningful phase curve for the 18.65, 0.948 or 0.901 d periods. Subsequently, Bonsack and Dyck (1983), Odell and Lebofsky (1984) and Kroll et al. (1987) found *no IR excess* in these stars, and Walker (1985) found that V 1046 Ori *is not an IRAS source*. Kroll et al. showed that Groote et al.'s IR excesses are probably instrumental artifacts due to the nonlinearity of their detector.

Borra and Landstreet (1979) discovered the variable magnetic field of V 1046 Ori, and Bohlender et al. (1987) made additional magnetic field measures. When the latter authors combined the two data sets, they found that the magnetic field strength varies with a period of $0\overset{d}{.}901195 \pm 0\overset{d}{.}000050$.

There have been reports that several other properties of V 1046 Ori vary with the $0\overset{d}{.}901$ period. Shore and Adelman (1981) discovered that the EWs of the Si III, Si IV and Al III lines in ultraviolet spectra of V 1046 Ori obtained with the *IUE* vary *in antiphase* to the He I line strengths. They also noted variations in the asymmetry of the C IV resonance line. They suggested that the RV variations measured from lines in the visible region of the spectrum might reflect the rotation of the star and not its orbital motion. More recently, Shore and Brown (1990) demostrated very convincingly that the strength of the UV resonance lines of C IV and Si IV vary with the 0.901 d period. Odell (1986) reported that the equivalent widths of both the Hα and He I $\lambda667.8$ nm lines vary with the $0\overset{d}{.}901$ period. Finally, Leone and Umana (1993) claim, based on their own observations and those by Drake et al. (1987) and Phillips and Lestrade (1988), that the 60 mm radio flux of V 1046 Ori varies with the $0\overset{d}{.}901$ period. However, the scatter about the supposedly sinusoidal $0\overset{d}{.}901$ curve is several times larger than the estimated errors of the observations.

We report here on a new spectroscopic and photometric study of V 1046 Ori that was designed to determine the true physical period(s) controlling the variations of the various observed quantities and check on its suspected binary nature. It is based on high-dispersion photographic spectra secured at the David Dunlap Observatory and electronic spectra obtained at the CFHT and KPNO and on unpublished photoelectric observations by Balona (1977) (kindly communicated to us by the author) and by one of us (DPS). In addition, we have analyzed all other available quantitative data on V 1046 Ori for periodicity.

2. Observations and reductions

2.1. Spectroscopy

We obtained the following new spectroscopic data for this study:

i. One 0.8 nm mm^{-1} and twenty-eight 1.2 nm mm^{-1} blue-violet photographic spectrograms exposed on baked IIa-O plates using the Cassegrain spectrograph on the 1.88-m reflector of the David Dunlap Observatory (DDO hereafter); and

– ii. twelve 0.48 nm mm^{-1} Reticon spectrograms of the Hα region obtained with the Canada-France-Hawaii Telescope (CFHT hereafter).

In addition, we have reanalyzed fifteen CCD spectrograms of the Hα and He I $\lambda667.8$ nm region obtained by Odell (1986) with the KPNO coudé feed telescope and the Hα profile obtained by Leone (1993) with the CCD spectrograph at the Cassegrain focus of the 2.5-m Isaac Newton Telescope at Observatorio del Roque del los Muchachos. Finally, Dr. J. P. Kaufmann generously sent us the mean RVs for nine spectrograms obtained by Groote (1978). The new spectroscopic observations and previously published RVs are summarized in Table 1. Here, and

Table 1. Journal of radial-velocity data of V1046 Ori

Source	Epoch (JD-2400000)	No. of RVs of primary	No. of RVs of secondary	Spectrograph	Dispersion (nm mm^{-1})
Plaskett & Pearce (1931)	24116-25310	5	0	1	4.9
Blaauw & van Albada (1963)	35447-35834	19	0	2	3.4
Groote (1978)	42819-42828	9	0	3	2.0
Morrell & Levato (1991)	43540-44992	10	0	8	6.0
This paper, DDO	44950-46074	28	27	4	1.2
	46037	1	1	4	0.8
This paper, CFHT	46039-46045	12	12	5	0.48
This paper, KPNO	44979-44983	15	12	6	1.47
This paper, Obs. del Roque	48259	1	1	7	0.98

Spectrographs: 1... Dominion Astrophysical Observatory 1.83-m reflector, Cassegrain prism spg.; 2... McDonald 2.08-m reflector, grating spg.; 3... ESO La Silla 1.52-m reflector, coude grating spg.; 4... David Dunlap 1.88-m reflector, Cassegrain grating spg.; 5... Canada-France-Hawaii 3.6-m reflector, grating spg. & a CCD camera; 6... Kitt Peak coude feed reflector, grating spg. & Fairchild CCD camera with 680 pixels; 7... Isaac Newton 2.5-m reflector, Intermediate-disp. Cassegrain grating spg. & GEC CCD; 8... Cerro Tololo 0.91-m reflector, grating spg.

elsewhere in this paper, whenever the observations were published with geocentric Julian dates (GJD hereafter), we have converted to heliocentric Julian dates (HJD) before using them in our analyses.

The DDO photographic spectra were scanned with the PDS 1010A microdensitometer at DDO, converted to intensities and rectified using the interactive program REDUCT (Gulliver 1976, Irwin 1978). The CFHT reticon spectra were reduced using a set of IDL procedures written by one of us (RWL) that subtract the bias from each spectrum, divide each by a flat field spectrum of equal intensity, calibrate the wavelength scale using exposures of a thorium-neon lamp taken at the beginning and end of the night, eliminate the 4/8 point pattern using an FFT filter, remove cosmic rays and blemishes, and rectify the spectrum to unit continuum. The KPNO CCD spectrograms were flat fielded by Odell and later rectified by Harmanec using the program SPEFO developed and kindly put at our disposal by the late Dr. J. Horn (see Škoda 1996).

2.2. Photometry

We compiled and analyzed all the available photometric, spectrophotometric and magnetic field data in order to explore the periodic variability of V 1046 Ori as thoroughly as possible. The individual observations were either compiled from the literature or obtained through the courtesy of authors who had not published them in the original papers. In addition, one of us (DPS) obtained new $uvby$ observations with the Automatic Photoelectric Telescope between 1992 and 1996. The complete set of observations used in this analysis is summarized in Table 2, and previously unpublished data is tabulated in Table 3.[1]

Before we could perform a period analysis on all the photometric data listed in Table 2, we had to transform the different data sets into one system. Fortunately, all the differential observations were secured relative to the nearby star HR 1891

(HD 37016), which has an optical energy distribution similar to V 1046 Ori's. We adopted the all-sky y magnitude of HR 1891 derived by Adelman and Pyper (1985), and the homogenized colour indices of HR 1891 given by Hauck and Mermilliod (1980) which resulted in the following $uvby$ magnitudes for HR 1891:

$$y = 6\overset{m}{.}251, b = 6\overset{m}{.}189, v = 6\overset{m}{.}227, u = 6\overset{m}{.}520.$$

These values were added to the respective magnitude differences V 1046 Ori − HR 1891. On two occasions, Johnson et al. (1966) observed V 1046 Ori and HR 1891 one after the other while doing all-sky photometry. We used the respective Johnson U and V magnitude differences to derive the Strömgren u and y magnitudes from them. We combined 56 individual differential U and V observations of V 1046 Ori by Balona (1977) into 9 normal points by averaging 4 to 7 individual observations obtained within a span of 0.03 d. Maitzen's (1981) all-sky $uvby$ observations were transformed into the standard Strömgren system by the author. We note that they differ systematically from the other data sets. We, therefore, allowed for automatic zero-point corrections during the least-square fits for this particular small data set. All other data sets turned out to be directly comparable. The mean values for V 1046 Ori, derived from our homogenization, agree very well with those given by Hauck and Mermilliod (1980).

3. Period analysis

3.1. Radial velocities

During preliminary inspection of the DDO photographic spectra, one of us (CTB) noted the presence of a narrow absorption component in the Mg II λ448.1 nm line that could be attributed to the secondary of the putative binary system because it shifted back and forth accross the primary's broader line. This prompted us to look for lines of the secondary's spectrum in all the other spectra at our disposal.

---

[1] Table 3 is only available in electronic form: see footnote on page 1.

Table 2. Journal of photometric, spectrophotometric and polarimetric observations of V1046 Ori used for period analyses

Source	Epoch (JD-2400000)	No. of obs.	No. of nights	Passbands	Instrument	Remarks
Johnson et al. (1966)	38670-38671	2	2	UBV	1	dif.
Balona (1977)	42770	9	1	U, V	2	dif.
Pedersen & Thomsen (1977)	42778-42820	7	7	$uvby$	3	all-sky
Maitzen (1981)	44197-44205	3	3	$uvby$	4	all-sky
Adelman and Pyper (1985)	44216-45987	21	21	$uvby$	5	dif.
	44568-44655	12	8	$u - b$	5	sphot.
this paper	48911-48966	18	18	$uvby$	6	dif.
	49261-49369	15	15	$uvby$	6	dif.
	49653-49689	16	16	$uvby$	6	dif.
	50060-50119	18	18	$uvby$	6	dif.
Perryman et al. (1997)	47914-49060	89	27	H_p	14	all-sky
Drake et al. (1987)	45883-46141	6	4	20 mm flux	7	
	45965-46141	5	3	60 mm flux	7	
	46136-46141	4	2	200 mm flux	7	
Phillips & Lestrade (1988)	47229	1	1	60 mm flux	8	
Leone & Umana (1993)	48306-48394	5	5	60 mm flux	7	
Pedersen & Thomsen (1977)	42799-42828	27	25	He I 4026	9	R-index
Pedersen (1979)	43059-43124	25	16	He I 4026	9	R-index
Borra & Landstreet (1979)	43442-43448	5	5	Hβ	10	circ. pol.
	43504-43511	5	5	Hβ	11	circ. pol.
	43558-43560	2	2	Hβ	10	circ. pol.
Bohlender et al. (1987)	44947-45308	23	18	Hβ	12	circ. pol.
	45718-45723	5	5	He I 5875	12	circ. pol.
Shore & Brown (1990)	44241-44958	23	7	C IV & Si IV	13	a-index

The instruments used: 1... Standard Johnson UBVRI photometry obtained at the Catalina Station of the Lunar and Planetary Laboratory; 2... Johnson U and V photometry secured at Sutherland, South Africa, with a 0.5-m reflector with a DC photometer and a strip-chart recorder; 3... All-sky instrumental Strömgren photometry obtained with the Danish 0.50-m reflector at ESO, La Silla; 4... All-sky Strömgren photometry transformed into the standard system, obtained with the Danish 0.50-m reflector at ESO, La Silla & EMI 6256A photomultiplier; 5... Strömgren photometry transformed into the standard system, obtained with the Kitt Peak National Observatory 0.41-m (No.4) reflector, and spectropho-tometric scans from the KPNO 0.92-m (No.1) reflector reduced to the same system; 6... Strömgren photometry transformed into the standard system, obtained with the 0.8-m Four-College Automatic Photoelectric Telescope; 7... radio flux observed very the VLA (Very Large Array) system; 8... radio flux observed with VLBI (very-long baseline interferometry); the diameter of the source was found to be smaller than $0\overset{''}{.}0005$; 9... a two-channel photometric ratio of the intensity of He I 4026 line and its neighouring continuum measured with spectrometers attached to the Danish 0.50-m telescope at La Silla and ESO 1.0-m telescope at Las Campanas and subsequently transformed into one system; 10.. Hβ line circular polarization measured at the 1.5-m Palomar reflector; 11.. Hβ line circular polarization measured at the du Pont 2.54-m reflector at Las Campanas; 12.. Hβ and He I 5875 circular polarization measured alternatively at the du Pont 2.54-m, 1.5-m Palomar reflector and 1.2-m reflector of the University of Western Ontario; 13.. a two-channel photometric ratio a of the intensity of C IV and Si IV UV resonance lines and their neighbouring continuum measured from the high-dispersion SWP spectra obtained with the IUE; the larger positive value of the index, the stronger absoption. 14.. the Hipparcos broad-band H_p magnitude converted to Johnson V with the help of a transformation formula derived by Harmanec (1998)

The list of spectral lines that are suitable for RV measurements in our spectra and their adopted wavelengths is tabulated in Table 4. We measured the RVs from the photographic spectra by fitting parabolae to the lower parts of the line profiles. The RVs of the narrow component in the Mg II λ448.1 nm line were measured by finding the position of its minimum intensity in the intensity tracings. We also measured the equivalent width, central intensity and full width at half maximum (EW, I_c and FWHM hereafter) of the He I λ447.1 nm line, the strongest He I line in our spectra. The results of these measurements are summarized in Table 5.[2] Since we find that different lines follow

different RV curves, we have tabulated the mean radial velocities for the H I and He I (singlet) lines, the He I (singlet) lines only, and the He I λ416.9 nm line from the primary spectrum separately along with the RVs for the narrow Mg II λ448.1 line in the secondary spectrum and the narrow Ca II K line.

The RVs of the Hα and He I λ667.8 nm lines in the KPNO spectra were measured with the program SPEFO mentioned above. The wavelength calibration of these spectra was corrected by measuring the stronger telluric water vapour lines. The results of these measures are tabulated in Table 6. The RVs of the main Hα profile as well as of a narrow secondary absorption were measured directly from plots of the reduced CFHT spectra.

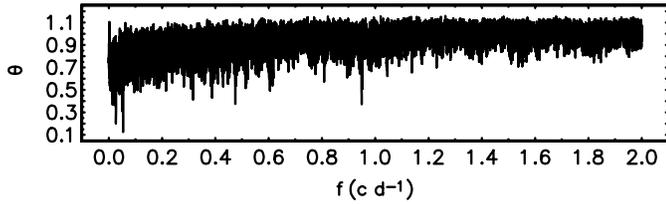[2] Table 5 is only available in electronic form: see footnote on page 1.

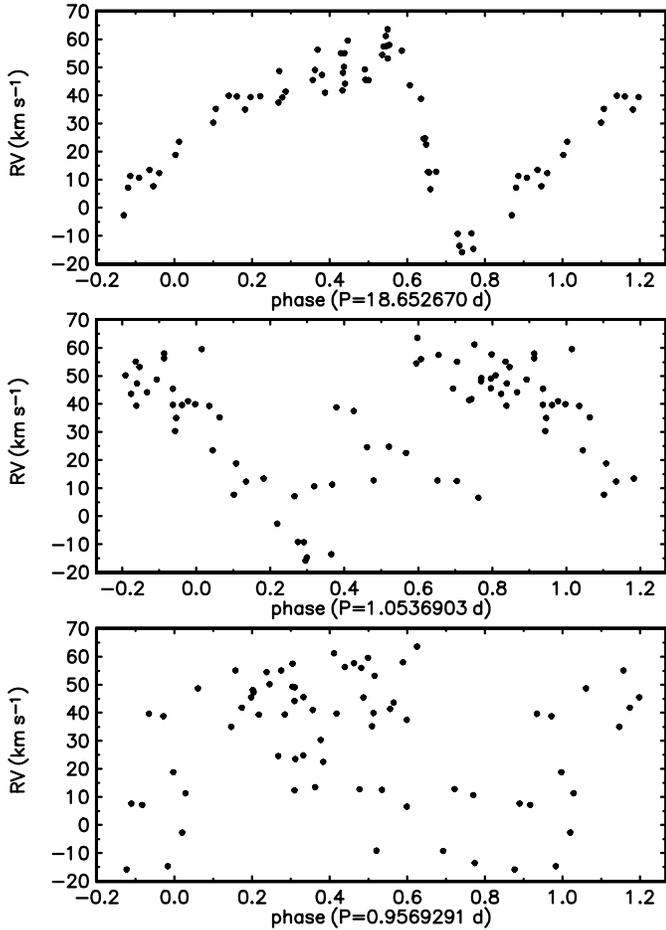**Fig. 1.** The PDM periodogram for 56 new RVs of the primary

Fig. 2. The phase plots of RVs for the $18^{\rm d}\!.65$ period and its one-day aliases

These results are tabulated in Table 7 along with the RV of the Hα profile and its secondary absorption core in Leone's (1993) line profile. The latter were measured directly from Fig. 1 of his paper and corrected to the heliocentric wavelength scale. The Julian date of the mid-exposure of this observation was kindly communicated to us by the author.

A quick scan of our new RV measures shows that the narrow component of the Mg II line (FWHM = 0.1 ± 0.02 nm) and similar narrow absorption features in Hα and the He I λ667.8 nm lines move in antiphase to the broad H I and He I lines with an amplitude of nearly 200 km s^{-1}. This eliminates any doubt about the duplicity of V 1046 Ori. It also indicates that Leone's (1993) interpretation of a single Hα profile, secured by chance at an elongation of the binary, and the models based on

Table 4. A list of spectral lines and wavelenghts used to the determination of radial velocities of V1046 Ori

Wavelength (nm)	Identification	Wavelength (nm)	Identification
667.8151	He I sgl	414.3759	He I sgl
656.2817	Hα	410.1737	Hδ
492.1929	He I sgl	400.9270	He I sgl
486.1332	Hβ	397.0074	H 7
448.1228	Mg II	393.3664	Ca II K
443.7549	He I sgl	388.9051	H 8
438.7928	He I sgl	383.5386	H 9
434.0468	Hγ	379.7900	H 10
416.8971	He I sgl		

this interpretation, are probably incorrect. We have reinterpreted this profile, as noted in the previous paragraph.

We employed Stellingwerf's (1978) phase dispersion minimization (or PDM) technique, using 10 phase bins and 4 "covers", to search for periods in the RV data because it has the advantage that it makes no *a priori* assumption about the shape of the phase curve. We started by analyzing the mean (or mean H I) velocities for the primary, since these are available for all of the data sets.

We first searched our 56 new RVs for periods between 0.5 and 5000 d. We used a frequency step $\Delta f = 0.05/\Delta T$, where ΔT is the time interval spanned by the data set. This ensures that no data point changes its position within the phase curve by more than $0^{\rm P}\!.05$ between adjacent frequencies and, therefore, that no significant period is missed in the search. The PDM ϑ periodogram is shown in Fig. 1. The deepest minima in this diagram correspond to the $18^{\rm d}\!.65$ period discovered by Blaauw and van Albada (1963) and its first overtone. The phase plots of the primary RVs for the $18^{\rm d}\!.65$ period and its best-fit one day aliases are shown in Fig. 2. The superiority of the longer period is obvious.

We therefore take as proven that V 1046 Ori is indeed a binary and that its orbital period is $18^{\rm d}\!.65$ as originally found. Groote's (1978) suggestion that the orbital period is $0^{\rm d}\!.948$ is firmly excluded by our data.

We tested the secular constancy of the orbital period by searching the primary RVs from the first and second approximately 10000 d of observations for periods between 17 and 20 d using a mesh ten times finer than the original search. That is, the maximum phase shift of a point between two adjacent periods was no more than $0^{\rm P}\!.005$. We also seached the complete set of primary RVs and all secondary RVs in the same way. The PDM spectra for these searches are shown in Fig. 3, which shows that all of the RVs can be reconciled with a period close to $18^{\rm d}\!.655$.

We calculated several exploratory orbital solutions to improve the value of the orbital period and to test the binary model. We used the FORTRAN program FOTEL (Hadrava 1990) kindly put at our disposal by the author. FOTEL is based on the simplex method of least-squares minimization and de-
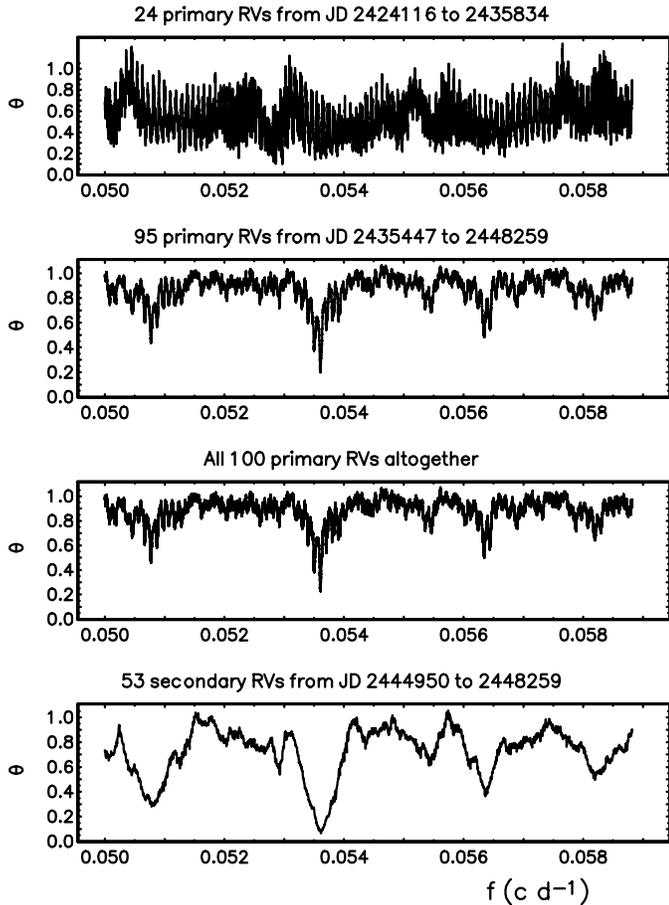
Fig. 3. The PDM ϑ periodogram in the neighbourhood of the $18\overset{d}{.}65$ period for various data subsets

rives the rms errors of individual elements from a covariance matrix. It is designed so that it can be used to solve for triple-star orbits, apsidal motion or a monotonic period change.

The RVs were weighted according to formula

$$w = 0.2QND^{-1}, \tag{1}$$

where N is the number of lines measured (1 to 14 in practice), D is the linear dispersion of the spectrogram in question(in nm mm^{-1}), and Q was set equal to 1 for photographic, and 2 for the electronic spectra. This means that weight of 1.0 corresponds to a RV based on the mean value of 5 spectral lines measured on a photographic spectrogram with dispersion of 1.0 nm mm^{-1}. Since it is not clear from Morrell and Levato's (1991) paper whether their spectra have a dispersion of 4.0 or 6.0 nm mm^{-1} and their RVs have large internal errors, we calculated their weights by assuming the linear dispersion was 6.0 nm mm^{-1}. In practice, the weights ranged from 0.167 to 3.25 over our entire data set.

We used our first exploratory fits to verify that separate solutions for the primary and secondary RVs yield identical orbital elements (P, e, ω, γ) within the limits of their respective errors. Next, we calculated orbital solutions for various suitably chosen local subsets of the data (with each spanning no more than 1000

Table 6. Radial velocities (in km s^{-1}) of the primary and secondary components of V 1046 Ori from the Kitt Peak National Observatory CCD spectrograms

HJD -2400000	RV$_1$ Hα	RV$_1$ He I 6678	RV$_2$ Hα	RV$_2$ He I 6678	RV$_2$ mean
44979.6615	41.8	65.3	–	–	–
44979.6885	48.1	72.9	-20.9	-18.8	-19.9
44979.7302	50.2	65.3	–	–	–
44979.7586	55.1	66.7	–	–	–
44979.7913	44.2	67.2	-27.8	-17.3	-22.5
44980.7433	49.3	70.0	-32.7	–	-32.7
44980.7704	45.6	59.5	-33.9	–	-33.9
44980.9187	45.4	60.4	-26.1	–	-26.1
44982.9068	43.6	44.0	-5.6	–	-5.6
44983.5790	24.6	32.4	21.2	26.0	23.6
44983.6408	24.8	20.4	30.3	35.0	32.6
44983.6901	22.5	23.5	30.9	38.1	34.5
44983.7797	12.7	24.1	30.5	45.6	38.0
44983.8349	12.5	13.1	34.3	48.8	41.5
44983.8960	6.5	16.8	40.8	60.5	50.6

Table 7. The Hα RVs of the primary and secondary component of V1046 Ori from the Canada-France-Hawaii and (the last line) Roque del los Muchachos CCD spectrograms

HJD -2400000	RV$_1$ (km s^{-1})	RV$_2$ (km s^{-1})
46039.831	48.7	-4.2
46039.981	39.3	-5.6
46041.882	47.3	-23.4
46042.028	41.0	-26.7
46042.794	55.1	-27.1
46043.121	59.6	-34.4
46044.785	54.5	-42.4
46044.849	57.5	-40.6
46044.951	61.2	-38.3
46045.000	57.7	-39.9
46045.051	53.2	-40.4
46045.121	58.0	-35.8
48259.464	37.5	5.7

days), with the period fixed. With one exception, discussed in the next paragraph, the velocity curves for the different subsets are in phase with each other, i.e., the epochs T are separated by an integral number of periods within the accuracy of the data. Thus there is no evidence of a secular period change.

The data set from the DAO (Plaskett and Pearce 1931) consisting of five radial velocities is the exception to the result reported above. Moreover, all the solutions for this small data set yielded a systemic velocity approximately 10 km s^{-1} higher than the other data sets. These discrepancies are due to the RV for 1925 January 15 (HJD 2424165.803). When it is omitted, the remaining DAO radial velocities fit a velocity curve with

the same phase and in the systemic velocity as the other data. V 1046 Ori was observed by Plaskett and Pearce on the same nights as the nearby star HD 37016. On the night in question, they quote the same RVs for both stars, which suggests that the published RV for V 1046 Ori may be incorrect. Upon our request, Dr. A.H. Batten re-measured this particular plate using the Arcturus oscilloscopic device at the DAO. He was able to measure six H and He lines and found a RV of -22 km s^{-1}. This value fits nicely our RV curve. According to Dr. Batten, Plaskett and Pearce (1931) probably omitted a minus sign in their published velocity for the plate in question. Since Dr. Batten used new wavelengths, we followed his recommendation and simply omitted this datum from all following analyses. As a precaution, we have also omitted a single RV from HJD 2444991.563 by Morrell and Levato (1991) because it has an unusually large residual (over 30 km s^{-1}) from the RV curve of the primary defined by the other observations.

Although our exploratory solutions of subsets of the data hint at very slow apsidal motion (ω growing from $110°$ at JD 2435600 to $117°$ at JD 2446000), the orbital solution was not improved by including apsidal motion. Moreover, the derived rate of apsidal motion is smaller than its error. Therefore we assume that the data can be satisfactorily described by one constant set of the orbital elements. Thus we used all of the primary (except the two mentioned above) and secondary RVs to determine an improved value for the orbital period.

We have tabulated the results from five different orbital solutions in Table 8 to show how the results are affected by various assumptions and our system for weighting the data.

Solution 1: The systemic velocity was determined separately for each spectrograph, defined in Table 1. Moreover, the systemic velocities were derived separately for the primary and secondary stars for each spectrograph. (Note that the single RV from spectrograph 7 was treated as though it belonged to the data set from spectrograph No. 5 in all similar solutions.)

Solution 2: The systemic velocities were determined separately for the individual spectrographs, but the binary components were assumed to have identical systemic velocities.

Solution 3: The systemic velocity was determined separately for the primary and secondary RVs, and any differences in the RV zero-points among the spectrographs were ignored.

Solution 4 This solution is identical to solution 3, but the radial velocities are given equal (unit) weights.

Solution 5: This solution is based on unequally weighted data, as described above, and assumes that the γ velocity is identical for both stars and all data sets.

Table 8 shows that the different solutions yield consistent values for the period, eccentricity and longitude of periastron. There is a large dispersion among the systemic velocities for the different spectrographs in solution 1 — especially for the secondary star. We believe that this is caused mainly by the non-uniform phase distribution of the data. We obtain more consistent results if we assume identical systemic velocities for the primary and secondary star (solution 2). The remaining differences among the γ velocities can be attributed to differences
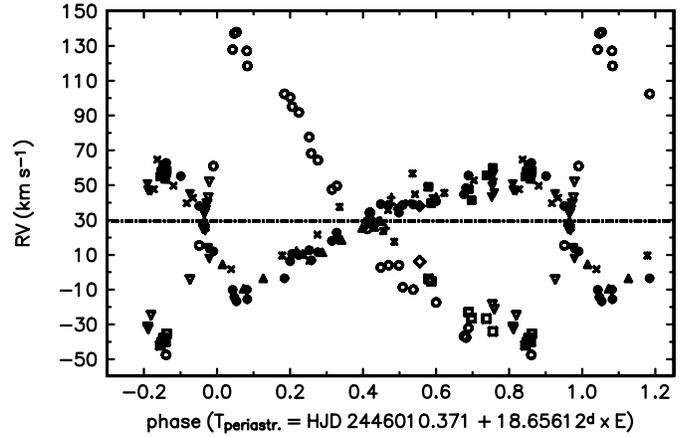

Fig. 4. Radial-velocity curves of the primary and secondary components of V 1046 Ori based on all available data and corresponding to solution 2. RVs of the secondary are shown by open symbols and different symbols are used for different data sets of Table 1

in the selection of lines used to obtain the mean RVs and the uneven phase distribution of the data in the smaller data sets.

We believe that solution 2 is probably the best of the solutions presented in Table 8, hence the preferred value for the orbital period is $P = 18\overset{d}{.}65612 \pm 0\overset{d}{.}00023$. The phase diagram for solution 2 is shown in Fig. 4. We caution, however, that it is not the best solution *for the remaining orbital elements of the system* since it is heavily weighted by velocities derived from the Balmer lines and these often give a lower orbital velocity than He I and metallic lines (cf., *e.g.*, Andersen et al. 1983). We will return to this point in Sect. 4.

One of the more striking features of Fig. 4 is the large scatter of the RVs of the primary star about the fitted curve; the RMS scatter about this curve is significantly larger than the mean errors of the RVs — especially for the velocities with lower mean errors. This prompted us to search for periodic variations in the $O - C$ residuals. We quickly found that the velocity residuals fit a single-wave curve with a full amplitude of about 9 km s^{-1} and a period of $0\overset{d}{.}9012$, i.e., the same period as the light and line-profile variations.

We therefore calculated additional trial orbital solutions for the primary RVs by formally modelling both the $18\overset{d}{.}65$ and $0\overset{d}{.}9012$ periods as the orbital motion in a triple system and assuming a "circular orbit" for the $0\overset{d}{.}9$ period. The results are summarized in Table 9. Solution 6 is based on data sets B and C, solution 7 on data sets D, E, F, and G, and solution 8 was calculated for the entire set of primary RVs, except the two omitted from solution 2. In each case we allowed the program to find different systemic velocities for the different data sets to preserve the sensitivity of the fit to the short period.

Both the early- and late-data groups indicate that the primary star velocity residuals vary with a period between $0\overset{d}{.}90118$ and $0\overset{d}{.}90121$, but when the the full data set are used, we obtain a somewhat shorter period, $0\overset{d}{.}901155 \pm 0\overset{d}{.}000005$. The differences between the periods derived for the early- and late-data groups and the full data set may not be significant considering

Table 8. Some orbital solutions for all 151 available mean RVs of both components of V1046 Ori (two primary RVs, the DAO RV obtained on 1925 January 15 and CTIO RV taken on HJD 2444991.563 were omitted from the solutions - see the text)

element	solution 1	solution 2	solution 3	solution 4	solution 5
P (d)	18.65625	18.65612	18.65596	18.65592	18.65595
rms error	0.00023	0.00023	0.00021	0.00029	0.00022
$T_{\mathrm{periastr.}}$	46010.475	46010.371	46010.390	46010.473	46010.385
rms error	0.063	0.068	0.075	0.082	0.074
e	0.469 ± 0.012	0.466 ± 0.014	0.468 ± 0.016	0.442 ± 0.014	0.468 ± 0.016
ω	116.0 ± 1.7	115.9 ± 1.9	116.1 ± 2.3	118.7 ± 2.2	116.1 ± 2.2
K_1 (km s^{-1})	35.47 ± 0.92	35.0 ± 1.0	34.4 ± 1.1	32.4 ± 1.3	34.4 ± 1.1
K_1/K_2 (km s^{-1})	0.391 ± 0.014	0.414 ± 0.017	0.397 ± 0.014	0.372 ± 0.016	0.400 ± 0.015
γ_1 (km s^{-1})	25.8 ± 3.5	26.1 ± 3.5	–	–	–
γ_2 (km s^{-1})	31.1 ± 1.3	31.3 ± 1.3	–	–	–
γ_3 (km s^{-1})	33.4 ± 1.3	33.4 ± 1.3	–	–	–
γ_4 (km s^{-1})	30.03 ± 0.70	29.71 ± 0.77	–	–	–
γ_5 (km s^{-1})	28.4 ± 1.4	28.54 ± 0.99	–	–	–
γ_6 (km s^{-1})	19.9 ± 1.2	27.6 ± 1.6	–	–	–
γ_8 (km s^{-1})	19.8 ± 3.6	19.4 ± 3.6	–	–	–
γ_{24} (km s^{-1})	26.0 ± 1.6	–	–	–	–
γ_{25} (km s^{-1})	32.2 ± 1.5	–	–	–	–
γ_{26} (km s^{-1})	38.4 ± 2.1	–	–	–	–
$\gamma_{\mathrm{prim.}}$	–	–	29.53 ± 0.63	28.11 ± 0.70	–
$\gamma_{\mathrm{sec.}}$	–	–	30.19 ± 0.99	29.5 ± 1.0	–
γ_{common}	–	–	–	–	29.60 ± 0.59
rms (km s^{-1})	4.35	4.79	5.14	6.94	5.14

Notes: Row "rms" contains the root-mean-square error of one observation of unit weight. The numbering of individual γ velocities corresponds to individual spectrographs as defined in column "No. of spg." in Table 1 for the primary; γ velocities 24 through 26 correspond to systemic velocities for the secondary component for the spectrographs 4, 5, and 6, respectively. All solutions are calculated for velocities weighted according to formula (1) with the exception of solution 4 which was calculated for *unweighted* data (see the text for details).

the errors for both the locally derived epochs and the fact the $0^{\mathrm{d}}9$ period is poorly defined by the older data. We shall return to this problem after we discuss our analyses of photometric and other data.

In summary, our principal conclusions from a period analysis of the RV data are:

– a. The orbital period of the V1046 Ori binary system is now well constrained at $18^{\mathrm{d}}.6561 \pm 0^{\mathrm{d}}.0002$. We have adopted this value for all subsequent analyses.
– b. The RV variation of V1046 Ori is *doubly* periodic. It is important to note (cf. solutions in Table 9), however, that the longer period is insensitive to the shorter period, lower amplitude variations.

3.2. Photometry

Here, our task was to improve the value of the already known $0^{\mathrm{d}}901$ period. Since previous observers have established that there is good phase coherence of the variations in all $uvby$ bandpasses, we used the FOTEL program to fit single-wave curves to the data. We first calculated separate solutions for each of the $uvby$ magnitudes and also for the $u - b$ index, for which additional data were available from Adelman and Pyper's spec-

trophotometric scans (cf. Table 2). The period was one of the free parameters in these solutions. The solutions converged to periods between $0^{\mathrm{d}}901173$ and $0^{\mathrm{d}}901177$ for the u, $u - b$ and v data (with errors ranging from $0^{\mathrm{d}}000002$ to $0^{\mathrm{d}}000006$), and to $0^{\mathrm{d}}901194$ and $0^{\mathrm{d}}901198$ (with similar errors) for the y and b data, respectively. The values for the optical and UV regions differ for more than the calculated errors and also have slightly, but significantly different epochs of the brightness maxima. The (improbable) possibility of a significantly different periodicity of light changes in different wavelengths should perhaps be kept in mind and further tested. However, for the moment, we consider this difference insignificant and adopt the mean period and epoch from these trial fits to obtain the following improved ephemeris to be adopted here:

$$T_{\mathrm{max.\ brightness}} = \mathrm{HJD}\ 2446010.3750 + 0^{\mathrm{d}}9011836 \times E. \quad (2)$$

For completeness, we checked the residuals from the light curve defined by this ephemeris for variations with the orbital period. There are none. In particular, the phases around the binary conjunctions predicted by the orbital solutions tabulated in Tables 8 and 9 are well covered by the data, but there is no evidence that V 1046 Ori is an eclipsing binary.

The period derived from the light variations is in good agreement with the period derived from the residuals of the more re-

Table 9. "Triple-star" orbital solutions for the primary velocities of old, new and all primary RVs of V1046 Ori, respectively. (Two RVs were omitted - see the text)

element	solution 6	solution 7	solution 8
$P_{orb.}$ (d)	18.65655	18.6539	18.65609
rms error	0.00038	0.0031	0.00024
$T_{periastr.}$	35824.02	46010.23	46010.337
rms error	0.27	0.17	0.076
e	0.409	0.485	0.473
rms error	0.029	0.019	0.014
ω (°)	111.8 ± 5.8	114.2 ± 2.8	114.8 ± 2.2
K_1 (km s^{-1})	31.7 ± 2.0	35.64 ± 0.82	34.75 ± 0.67
γ_1 (km s^{-1})	–	–	25.7 ± 2.5
γ_2 (km s^{-1})	32.0 ± 1.2	–	31.4 ± 1.2
γ_3 (km s^{-1})	32.9 ± 1.2	–	33.34 ± 0.91
γ_4 (km s^{-1})	–	29.04 ± 0.51	29.02 ± 0.49
γ_5 (km s^{-1})	–	27.5 ± 1.4	28.1 ± 1.4
γ_6 (km s^{-1})	–	20.1 ± 1.6	20.8 ± 1.3
γ_8 (km s^{-1})	–	–	18.5 ± 3.4
$P_{rot.}$ (d)	0.901184	0.901208	0.9011547
rms error (d)	0.000026	0.000043	0.0000051
$T_{max.RV}$	35820.70	46009.846	46009.805
rms error	0.14	0.037	0.021
K_3 (km s^{-1})	1.9 ± 1.1	3.94 ± 0.72	4.04 ± 0.60
rms (km s^{-1})	3.28	2.74	3.42
No. of RVs	28	57	98

Notes: Row "r.m.s." contains the root-mean-square error of one observation of unit weight. The numbering of individual γ velocities corresponds to individual spectrographs as defined in column "No. of spg." in Table 1. All solutions are calculated for velocities weighted according to formula (1).

Table 10. Final orbital solutions for V1046 Ori. The value of the orbital period was fixed at $18\overset{d}{.}6561$. Solution 9 is based on He I singlet RVs for the primary prewhitened for the $0\overset{d}{.}901$ residual RV variation and on all available secondary RVs. Solution 10 which we adopt to define the best orbital elements of the system is similar to solution 9 but based on the net orbital He I 416.9 line RV for the primary plus all available RVs for the secondary. All epochs are in HJD-2400000

element	solution 9	solution 10
$T_{periastr.}$	46010.434	46010.461
rms error	0.067	0.080
$T_{l.conj.}$ 46009.956	46009.978	
$T_{min.RV}$ 46011.596	46011.627	
$T_{max.RV}$ 46007.153	46007.160	
e	0.470 ± 0.012	0.468 ± 0.014
ω (°)	118.2 ± 2.0	118.3 ± 2.4
K_1 (km s^{-1})	42.95 ± 0.94	45.8 ± 2.2
K_2 (km s^{-1})	87.0 ± 2.9	87.4 ± 6.0
γ_4 (km s^{-1})	33.30 ± 0.78	42.9 ± 1.9
γ_6 (km s^{-1})	29.3 ± 1.2	–
$\gamma_{sec.}$ (km s^{-1})	29.69 ± 0.95	30.09 ± 0.93
$M_1\sin^3 i$ ($\mathcal{M}_\odot$)	1.955	2.072
$M_2\sin^3 i$ ($\mathcal{M}_\odot$)	0.965	1.087
$A \sin i$ (R$_\odot$)	42.3	43.4
rms (km s^{-1})	4.77	6.63
No. of RVs	97	81

Notes: Row "rms" contains the root-mean-square error of one observation of unit weight. The numbering of individual γ velocities corresponds to individual spectrographs as defined in column "No. of spg." in Table 1. All solutions are calculated for velocities weighted according to formula (1).

cent data from the primary's long-period velocity curve and has a smaller error. Thus we have adopted the ephemeris to compare the various observed properties that vary with the short period.

4. Final spectroscopic orbital elements

RVs measured from H I and He I lines in the spectra of double-line spectroscopic binaries often define different velocity curves because of pair blending and other effects. We see this effect in V 1046 Ori. The velocity dispersion among lines from spectra obtained near the velocity extrema is much larger than at other phases and the differences between the H I and He I singlet mean RVs varies in a similar manner[3]. There are, however, no systematic velocity differences among individual H I lines or among individual He I singlet lines. The singlet He I lines, especially the weak ones such as λ416.9 nm, which is unobservable in photographic spectra of rapidly rotating, normal B

stars, have the largest velocity amplitude, and we shall adopt their velocities as the most representative for the orbital motion of the helium-strong primary.

We calculated a "triple-star" solution for the RVs measured from the primary He I singlet lines, with the periods fixed at the values derived earlier, $18\overset{d}{.}6561$ and $0\overset{d}{.}9011836$. We then used the elements obtained from this solution to prewhiten the primary RVs by removing the short-period oscillation. Solution 9 in Table 10 was obtained by combining the prewhitened primary RVs with the RVs of the secondary star. For this solution, we assumed that the primary and secondary star have the same systemic velocity and allowed the program to solve for different γ-velocities for the primary RVs obtained with spectrographs 4 & 6 because each of these sets is based on different He I lines.

Our final solution 10 is similar to solution 9 but based solely on the RV of the He I 416.9 line (which we assume comes purely from the He-enriched atmosphere of the primary and is, therefore best suited to characterize its orbital motion) combined with all RVs of the secondary. Note that apart from a higher K_1 value, the elements from solutions 9 and 10, including the orbital eccentricity, are in good agreement with those obtained in the solutions tabulated in Tables 8 and 9.

---

[3] It is a bit disturbing that these effects are larger at velocity maximum than at the minimum. Since we can't explain this effect, we'll ignore it, but the orbital elements may require refinement once it is understood.

5. Basic physical properties of the system

5.1. Phase relations among the short-period variations

We calculated least-squares fits to the calibrated differential $uvby\beta$ photometry from instruments 5 & 6 (cf. Table 2) to obtain quantitative information needed to estimate the physical properties of V 1046 Ori. There are no statistically significant phase-dependent variations in either $b - y$ and m_1. The results for the fits to the other bandpasses and colours are tabulated in Table 11. The maxima and minima do not occur at exactly the same phases in the different colours and bandpasses; they appear to occur later in the u band than in the visual.

We also investigated the radio light curves (cf. Table 2)[4]. Leone and Umana (1993) have previously noted that the radio flux seems to vary roughly sinusoidally with the $0\overset{d}{.}9$ period. We find that it fits a period of $0\overset{d}{.}946861 \pm 0\overset{d}{.}000023$ period better; the rms is 0.28 compared to 0.34 for the $0\overset{d}{.}901$ period. We note, however, that the larger scatter with respect to the $0\overset{d}{.}901$ period is due to a single observation by Phillips and Lestrade (1988). When this observation is omitted, the $0\overset{d}{.}901$ period fits the data better. More radio observations would clearly be desirable. A least-squares fit to the 60-mm radio light curve for the $0\overset{d}{.}901$ period is given in Table 11. Fig. 5 compares the phase plots of the various quantities. The radio flux curve is in phase with the u band light curve.

Bohlender et al. (1987) derived a period of $0\overset{d}{.}901195 \pm 0\overset{d}{.}000050$ from all the magnetic field measurements. This is identical to the period we derive from the photometry within the errors of the determinations. The negative magnetic extremum coincides with the c_1 maximum (cf. Fig. 5 and Table 11).

The interpretation of Pedersen and Thomsen's (1977) and Pedersen's (1979) R-index observations is not straightforward because the radial velocity of the primary star must affect the measured value. The primary's RV amplitude corresponds to a wavelength shift of more than 0.1 nm at the He I λ402.6 nm line while secondary line has a wavelength shift of more than 0.2 nm. This is bound to have some effect on the R-index because the line intensity is integrated over a bandwidth of only 0.7 nm, and the RV variations were neglected when the data were reduced. As the original investigators noted, both data sets define a double-wave curve with a 0.948366 d period, but the scatter is smaller for the 0.901 d period. The R-index variation with this period is in phase with the EW, FWHM and I_c variations of the He I λ447.1 nm line. Both of these triplet He I lines are strongest near the light maxima, as are the He I λ667.8 nm and He I λ416.9 nm singlet lines (cf. some examples in Fig. 5).

On the other hand, the small number of Hγ EWs that we measured from the DDO spectra at various phases of the $0\overset{d}{.}901$ period and the two Hγ EWs published by Walborn (1983) and Klochkova (1991) indicate that Hγ is strongest at light minimum. This is confirmed by the β index photometry of Adelman and Pyper (1985) (cf. Fig. 5). Shore and Adelman (1981)

reported similar behaviour for some lines in the vacuum ultraviolet. This is now well documented by the so-called a-index measurements of line strengths for the C IV and Si IV UV resonance doublets by Shore and Brown (1990). Table 11 and Fig. 5 show that these lines vary exactly in antiphase with the c_1 index.

We investigated the phasing of the RV residuals of the H I and He I singlet line RVs from our high-dispersion spectra separately. The results for the mean H I and He I singlet RV residuals are given in Table 11 and a similar result for the weak He I λ416.9 nm singlet line is also shown in the form of a phase diagram in Fig. 5. The $0\overset{d}{.}9$ variation is present in all three data sets. The H I and He I residual velocity curves are *in phase* and their maxima precede the light minimum by about $0\overset{P}{.}25$.

We note in passing that the Hα line profile also appears to vary with the $0\overset{d}{.}9$ period. There is emission in the red wing of the line around phase $0\overset{P}{.}0$ and in the blue wing around phase $0\overset{P}{.}5$. The peak intensity of the stronger R peak of the emission is also plotted vs. $0\overset{d}{.}9$ phase in Fig. 5.

5.2. Basic physical properties of the primary

While our data are not ideal for deriving the basic physical elements of both stars, they are sufficient to allow us to restrict their range to the point where we can outline a self-consistent model for the system.

Effective temperature and gravity: The published estimates for the effective temperature and gravity of the primary star of V 1046 Ori are summarized in Table 12 along with the estimates of the reddening and chemical composition. With two notable exceptions, everyone agrees that the temperature is about 20000 K. Everyone agrees that the continuum energy distribution is essentially identical to that of normal stars. Thus we feel justified in using Napiwotzki et al.'s (1993) accurate calibrations of Strömgren colours for normal stars to estimate the effective temperature. The variations of the $u - b$ and $b - y$ colours derived from our least squares fits to the observations translate into a $T_{\rm eff}$ variation from 19000 K to 19600 K. Adopting $E(b - y) = 0\overset{m}{.}06$ (Adelman and Pyper 1985) and using Balona's (1994) recent calibration based on c_1 and E(b-y), we obtain $T_{\rm eff}$ = 21100 K.

Using our mean $c_1 = 0\overset{m}{.}148$ and $\beta = 2.645$, we obtain $T_{\rm eff}$ = 20900 K and $\log g \sim 3.95$ from the Moon and Dworetsky (1985) calibration. When we apply the correction recommended by Napiwotzki et al. (1993) we find $\log g = 4.1$. Balona's (1984) calibration yields $\log g = 3.722$, which again leads to $\log g = 4.1$ when it is corrected according to Fig. 17 of Napiwotzki et al. (1993). Since these estimates are in reasonable agreement with the other determinations tabulated in Table 12, we adopt

$$\log g = 4.1 \pm 0.2.$$

The duplicity of V 1046 Ori obviously affects the observed continuum energy distribution, hence the $T_{\rm eff}$ derived from it. There are two contrasting effects. First, the composite energy distribution is redder than that of the primary. This causes $T_{\rm eff}$ to be underestimated. On the other hand, the change in the energy distribution may cause the reddening to be overestimated, and

---

[4] Note that there is a misprint in Table 1 of Leone and Umana (1993). The correct time for their first observation is GJD 2448306.688, i.e. HJD 2448306.690 (F. Leone, priv. comm.).

Table 11. Least-squares fits to various observed quantities of V1046 Ori which vary with the $0^{\rm d}.9011836$ period. The period was kept fixed in all fits. Depending on the character of the phase curve, sinusoidal or non-sinusoidal fit was calculated. This is denoted by letters "S" or "N", respectively, in column "Fit". Column "rms" contains a rms error of one observation for the respective fit and in respective units

Observable	Mean value	Semiamplitude	$T_{\rm max.}$	$T_{\rm min.}$	Fit	rms
u	6.7587± 0.0006	0.0156± 0.0005	46010.425± 0.008	46010.876	S	0.0063
v	6.5603± 0.0005	0.0081± 0.0009	46010.290± 0.014	46010.741	S	0.0053
b	6.5123± 0.0005	0.0085± 0.0009	46010.357± 0.013	46010.808	S	0.0052
y	6.5670± 0.0005	0.0075± 0.0010	46010.367± 0.013	46010.817	S	0.0070
b-y	-0.0571± 0.0005	0.0006± 0.0172	–	–	S	0.0052
u-b	0.2458± 0.0006	0.0084± 0.0010	46010.460± 0.014	46010.911	S	0.0061
c_1	0.1497± 0.0012	0.0158± 0.0010	46010.499± 0.015	46010.950	S	0.0117
m_1	0.1052± 0.0010	0.0034± 0.0040	46010.971± 0.060	46010.520	S	0.0094
β	2.6454± 0.0016	0.0071± 0.0397	46010.883± 0.042	46010.432	S	0.0068
60-mm flux	2.02± 0.11	0.440± 0.003	46010.429± 0.052	46010.880	S	0.35
R-index	0.5064± 0.0003	0.0111± 0.0004	46010.515± 0.005	46010.965	N	0.0020
a(C IV)	0.2419± 0.0099	0.1382± 0.0011	46010.974± 0.014	46010.523	S	0.0457
a(Si IV)	0.5103± 0.0077	0.1008± 0.0011	46010.971± 0.015	46010.520	S	0.0354
$B_{\rm eff}$	-1264± 69	985± 104	46010.938± 0.015	46010.487	S	431
EW He 667.8	0.0976± 0.013	0.068± 0.006	46010.327± 0.042	46010.777	S	0.045
EW He 447.1	0.1855± 0.028	0.378± 0.009	46010.428± 0.016	46010.878	S	0.140
I_c He 447.1	0.736± 0.002	0.022± 0.002	46010.977± 0.020	46010.527	S	0.009
I_c He 416.9	0.912± 0.002	0.015± 0.009	46010.886± 0.033	46010.436	S	0.011
O-C RV He I sgl.	–	6.8± 1.3	46010.747± 0.025	46010.296	S	3.70
O-C RV H I	–	3.4± 0.8	46010.674± 0.030	46010.223	S	2.28
O-C RV He I 416.9	–	14.7± 3.5	46010.723± 0.028	46010.272	S	8.55
O-C RV He I 447.1	–	1.4± 1.4	46010.859± 0.177	46010.408	S	4.16

this will cause the $T_{\rm eff}$ to be overestimated. We expect the first effect to be larger, so we adopt

$$T_{\rm eff} = 21000\,{\rm K, i.e.,} \log T_{\rm eff} = 4.322$$

as the most probable $T_{\rm eff}$, but we admit a conservative range of uncertainty from 19000 K to 24000 K.

Radius and mass: We estimate that $V_0 = 6^{\rm m}.4 \pm 0^{\rm m}.1$ taking into account the uncertainty in the exact value of $E(B-V)$. The Hipparcos parallax of V 1046 Ori, published by Perryman et al. (1997), is $0''.00268 \pm 0''.00098$. This implies the distance modulus of 7.86, with the range from 7.18 to 8.85. This agrees with the results of Jung (1970), who derived a distance modulus of 7.96 for V 1046 Ori from a statistical study of proper motions and radial velocities, and Wolff (1990), who obtained 7.7 ± 0.5 for the distance modulus of Ori OB1C association. Adopting the Hipparcos result, one gets the absolute visual magnitude of the binary in the range $-2^{\rm m}.6 \le M_{V(1+2)} \le -0^{\rm m}.7$. Wolff derived $M_V = -2^{\rm m}.27$ from the EW of Hγ and c_0. We estimate that the secondary is about $1^{\rm m}.0$ fainter than the primary in V. This implies that the system is $0^{\rm m}.36$ brighter than the primary alone, so that

$$-2^{\rm m}.2 \le M_{V1} \le -0^{\rm m}.3.$$

We adopt $M_{V1} = -1^{\rm m}.1$ as the most probable value within these limits, based on our mean y value, corrected by $0^{\rm m}.18$ for interstellar absorption and $0^{\rm m}.36$ for the light of the secondary, and the Hipparcos parallax.

The bolometric correction for $T_{\rm eff} = 21000$ K (Code et al. 1976) is $-2^{\rm m}.12$. This implies $M_{bol1} = -3^{\rm m}.2$, with possible values ranging from $-3^{\rm m}.9$ to $-2^{\rm m}.7$. The radius of the primary R_1 then lies between 1.9 and 4.6 R$_\odot$ with the most likely value being

$$R_1 = 2.8 R_\odot.$$

The ranges of uncertainty in R and $\log g$ allow primary masses in the range $1.1 \le \mathcal{M}_1 \le 15\,\mathcal{M}_\odot$, with

$$\mathcal{M}_1 = 3.5\,\mathcal{M}_\odot$$

corresponding to our most likely values. The "most probable" values of the mass and radius are in a complete disagreement with the observed spectrum.

The discrepancy is caused by our application of single-star calibrations to a composite spectrum. The problem is compounded by the variations of one of the spectra. The effects of these problems can be seen by using Millward and Walker's (1985) calibration to derive M_V from the EW of Hγ. The extrema of the Hγ EWs, derived from a least squares fit to our data, correspond to M_V changing from $-2^{\rm m}.88$ to $-2^{\rm m}.38$, but the observed variability in V is only $0^{\rm m}.02$! Note that Wolff's estimate for M_V is based primarily on the EW of Hγ. Lester's (1972) differential determination of the primary's basic properties relative to the nearby star HD 37016 must fail for the same reason, *and* because Millward and Walker (1985) found that HD 37016 is also a double-lined spectroscopic binary.
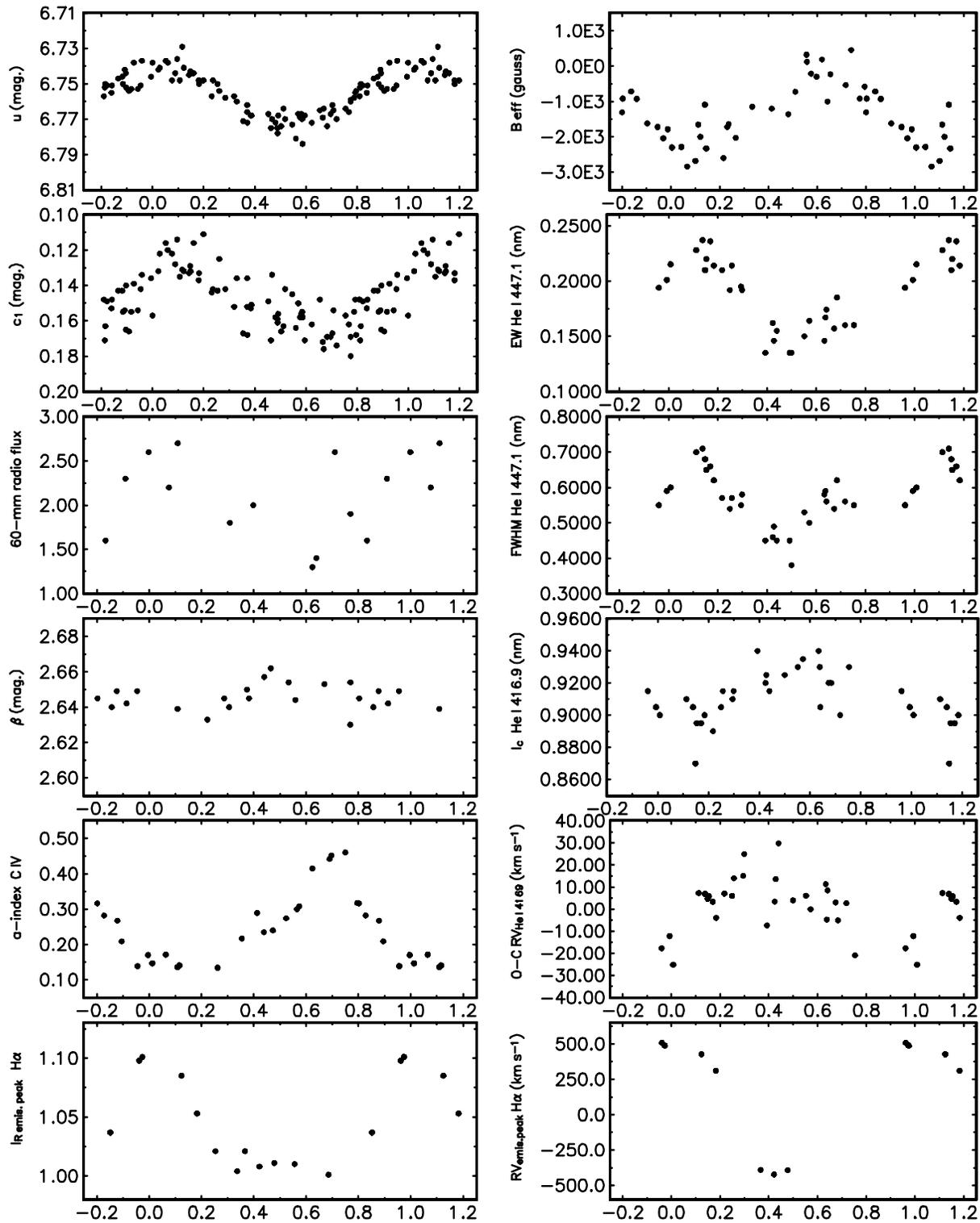
phase (HJD 2446010.375 + 0.9011836^d × E)

Fig. 5. Phase-locked variations of various observables with the $0^d.9011836$ period

Pending detailed line-profile modelling for both components based on high S/N spectra, we shall assume that the primary has the mass and radius normal for its effective temperature. Using Harmanec's (1988) formulae (3) and (4), we then

Table 12. Various determinations of the effective temperature T_{eff}, gravity acceleration g, reddening and chemical composition for the primary component of V1046 Ori

$T_{\rm eff}$ (K)	log g (CGS)	E(B-V)	N(He)/N(H)	Source	Notes
20000	4.0 assumed	$0\overset{\rm m}{.}09$	solar	Schild and Chaffee (1971)	1
21000	4.4	$0\overset{\rm m}{.}06$	0.19 ± 0.05	Lester (1972)	2
18000 ± 800	4.0 assumed	–	solar	Shore and Adelman (1981)	3
20000	4.0 assumed	$0\overset{\rm m}{.}086$	solar	Adelman and Pyper (1985)	4
24500 ± 500	4.0	–	–	Klochkova (1985)	5
20000	3.4	–	0.25	Odell (1986)	6
20300	3.9	–	–	Wolff (1990)	7
23750 ± 1250	4.0 assumed?	$0\overset{\rm m}{.}062$	–	Shore and Brown (1990)	8
20450 ± 450	4.15 ± 0.05	–	–	Bychkov (1991)	9

Notes: 1... energy distribution from photoelectric scans reduced to the Oke and Schild (1970) absolute calibration of Vega and from a comparison with the Kurucz model atmospheres for log g = 4.0; spectral class B2 IV based on 8.5 nm mm^{-1} spectra from Mt. Hopkins 1.5-m reflector; 2... from Schild and Chaffee's scans re-reduced to Hayes (1970) calibration of Vega and from 0.8 nm mm^{-1} photographic spectra from the McDonald 2.0-m reflector, based on comparison with Klinglesmith's (1971) model atmospheres for various chemical compositions and a detailed line-profile fitting for a number of spectral lines 3... from a comparison of the UV Si III and Si IV line strengths with Kamp's (1978) theoretical Si line profile strengths. 4... from the energy distribution obtained at many phases of the 0.901-d period with the HCO scanner attached to the Kitt Peak National Observatory 0.92-m No. 1 telescope and compared to solar composition log g = 4 Kurucz's model atmospheres; E(b-y)=$0\overset{\rm m}{.}06$ was derived and the E(B-V) quoted here was estimated as E(b-y)/0.7; 5... based on 0.9 nm mm^{-1} photographic spectra from the 6-m telescope, from the measured equivalent widths of the Balmer lines calibrated on normal stars; 6... from the phase-resolved (0.901-d period) analysis of the 1.7 nm mm^{-1} CCD spectra of Hα and He I 667.8 lines obtained with the coudé feed spectrograph of the Kitt Peak telescope, compared to Odell and Voels (1986) model atmospheres for various chemical compositions. 7... measurements of the Hγ line on CCD spectra from the Kitt Peak coudé feed telescope and previously published Strömgren photometry of the Balmer discontinuity were combined with Kurucz models of stellar atmospheres and several sets of evolutionary models; mass of 7.5 $\mathcal{M}_\odot$ and M$_{\rm bol}$ = $-4\overset{\rm m}{.}27$ and M$_{\rm V}$ = $-2\overset{\rm m}{.}27 \pm 0\overset{\rm m}{.}01$ were also derived; 8... from a comparison of low-dispersion IUE spectra with Kurucz's model atmospheres using E(B-V)=$0\overset{\rm m}{.}062$; 9... from a detailed analysis of the Balmer lines from 0.9 nm mm^{-1} photographic spectra obtained with the 6-m telescope, based on author's own calibrations for 76 normal and CP stars; M$_{\rm bol}$ = $-3\overset{\rm m}{.}52$ to $-3\overset{\rm m}{.}84$ and M$_{\rm V}$ = $-1\overset{\rm m}{.}60$ were also derived.

obtain

$$\mathcal{M}_1 = 7.2 \ \mathcal{M}_\odot, \ \text{and} \ R_1 = 3.9 \ R_\odot$$

for our best estimate of $T_{\rm eff}$.

Orbital inclination and projected rotation velocity: Solution 10 implies that the orbital inclination $i_{\rm orb.} = 41°.3$ for $\mathcal{M}_1$= 7.2 $\mathcal{M}_\odot$. If we assume that the inclination i of the primary's rotational axis is equal to $i_{\rm orb.}$ and adopt the $0\overset{\rm d}{.}901$ period as the rotational period, then the relation $v \sin i = 50.633 R P_{\rm rot.}^{-1} \sin i$ gives $v \sin i$ = 145 km s^{-1}. This is in a reasonable agreement with the width of all stronger He I lines in our spectra as well as with the estimates of $v \sin i$ by Odell (1986): 130 km s^{-1}, Walborn (1983): 170 km s^{-1} and McNamara and Larsson (1962): 170 km s^{-1}. However, several investigators have reported much lower values: for instance, $\leq$ 45 km s^{-1} (Levato 1975), 83 km s^{-1} (Klochkova 1985) and 85 km s^{-1} (Bychkov 1991). Notably, these low values fit better our observed profiles of the He I 416.9 line which call for $v \sin i$ of about 90 km s^{-1}. Note also that Lester (1972) obtained a wide range of $v \sin i$ for individual spectral lines of V 1046 Ori. These facts must be somehow related to an uneven distribution of the line intensities accross the observed stellar disk.

5.3. Dimensions of the binary system

For the orbital inclination estimated above, the semi-major axis of the binary orbit is $A = 65.8$ R$_\odot$, the separation of the stars at periastron is 35.0 R$_\odot$ and the equivalents to the Roche lobes at periastron have radii of 15.2 R$_\odot$ and 11.1 R$_\odot$. Phillips and Lestrade (1988) estimated that the projected diameter of the radio source must be $< 0''.0005$, *i.e.*, its radius is < 20 R$_\odot$ for distance $d = 390$ pc (Jung 1970). This means that, even at periastron, the radio source can probably be accomodated within the limit of dynamical stability around the primary.

If the rotation and revolution of the primary were synchronized at periastron as is observed for the majority of spectroscopic binaries with eccentric orbits (cf., e.g., Harmanec 1988), the rotation period would be $5\overset{\rm d}{.}97$. Clearly the primary's rotation period is much shorter than this.

5.4. Estimated properties of the secondary star

The mass ratio $\mathcal{M}_2/\mathcal{M}_1 = 0.525$ from solution 10 and the primary mass adopted above yield

$$\mathcal{M}_2 = 3.78 \ \mathcal{M}_\odot$$

for the mass of the secondary. This is the mass of a normal B6-B7 dwarf. This is consistent with our spectra. The radius of a

B6-7 dwarf is about 2.7 $R_\odot$. Such a star would be about $2^m_.0$ fainter than the primary in the V band. The 0.1 nm FWHM of the secondary's Mg II line implies $v_2 \sin i \sim 32$ km s^{-1}, *i.e.*, $v_2 \sim 48$ km s^{-1}. If the the secondary was rotating synchronously at periastron, its radius would be 5.7 $R_\odot$, which is well inside the radius of its Roche lobe at periastron. A secondary with this radius would be too bright relative to the primary to be consistent with the line strength ratios we observe in our spectra. Thus we conclude that the secondary is most probably a B6III-IV star that is rotating more rapidly than the synchronous velocity at periastron.

6. Rapid variations of the primary

Accurate mutual phasing of many various observables which vary with the – presumably rotational – period of $0^d_.901$ should – in principle – allow one to elaborate on the oblique rotator model of these variations. In spite of the large observational effort and progress in the analysis we feel, however, that new high-S/N spectral observations will still be needed to elaborate on the findings presented here. For this reason, we postpone an attempt at the quantitative modelling of the rapid changes for a separate study.

Here, we only present the following remark:

An inspection of Odell and Voels' (1986) tables of the theoretical EWs in He enriched atmospheres shows that, just in the temperature range near 20000 K we are interested in, the EW of the He I λ447.1 nm increases very steeply with the temperature, the EW of the He I λ667.8 nm line also increases but less steeply while the EW of the Balmer lines *decreases* with increasing temperature. We note that the observed behaviour is in an excellent qualitative agreement with the idea that the apparent T_{eff} varies cyclically as the primary rotates around its axis. At light maxima, the star is also bluest and the EWs of He lines attain their maxima while the strength of Balmer lines is at minimum (cf. Fig. 5). We stress that this remark is only a qualitative description of the situation which needs to be tested quantitatively in the future.

In passing we note that the periodic rapid variations could formally be also described as a non-radial pulsational mode with $m = $-1 (or $m = $-2 if the true period of rotation would be $1^d_.8$). This may have some relevance to the on-going discussion on the nature of rapid light and line-profile variations in "classical" Be stars.

7. Puzzles?

Fig. 6 is a plot of the RV of the supposedly interstellar Ca II K line from the DDO photographic spectra versus phase of the $18^d_.65$ period. One may suspect the presence of low-amplitude orbital RV variations. This suspicion should be tested through accurate RV measurements on future electronic spectra since it would represent some evidence of circumstellar matter around the whole binary.

We note a very puzzling near-coincidence between one of the 1-d aliases to the $18^d_.65$ orbital period, $0^d_.946665$, and syn-
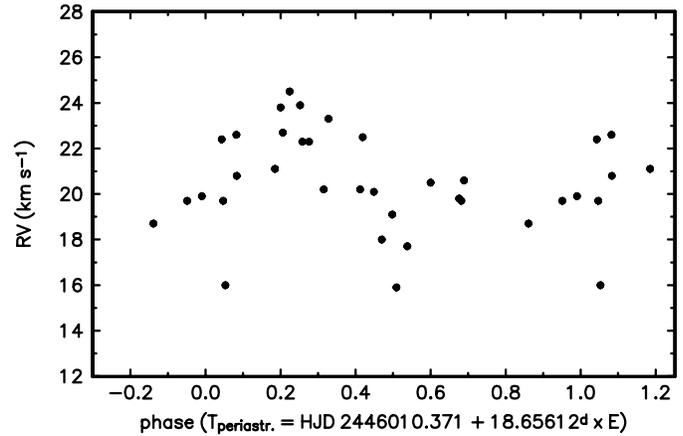

Fig. 6. Orbital RV variation of the "interstellar' Ca II K line of V 1046 Ori

odic rotational period of the primary, $0^d_.946924$. At present, we have no clear explanation for this fact. Quite possibly, it tells something important about the present dynamic state of the binary system, although it can also be viewed as a pure coincidence. In any case, it explains why different investigators were able to fold various observed quantities with several different periods.

References

Adelman S.J., Pyper D.M., 1985, A&AS 62, 279
Andersen J., Clausen J.V., Gimenéz A., Nordström B., 1983, A&A 128, 17
Balona L.A., 1977, Mem.R.Astron.Soc. 84, 101 and priv. com.
Balona L.A., 1984, MNRAS 211, 973
Balona L.A., 1994, MNRAS 268, 119
Blaauw A., van Albada T.S., 1963, ApJ 137, 791
Bohlender D.A., Brown D.N., Landstreet J.D., Thompson I.B., 1987, ApJ 323, 325
Bonsack W.K., Dyck H.M., 1983, A&A 125, 29
Borra E.F., Landstreet J.D., 1979, ApJ 228, 809
Bychkov V.D., 1991, Com. Special Astrophys. Obs. 66, 101
Code A.D., Davis J., Bless R.C., Hanbury Brown R., 1976, ApJ 203, 417

Drake S.A., Abbott D.C., Bastian T.S., Bieging J.H., Churchwell E., Dulk G., Linsky J.L., 1987, ApJ 322, 902

Groote D., 1978, Mitt. Astron. Gesellschaft No. 43, 263

Groote D., Kaufmann J.P., 1983, A&AS 53, 91

Groote D., Hunger K., Schultz G.V., 1980, A&A 83, L5

Gulliver, A., 1976, Ph.D. thesis, University of Toronto.

Hadrava P., 1990, Contr. Astron. Obs. Skalnaté Pleso 20, 23

Harmanec P., 1988, Bull.Astron.Inst.Czechosl. 39, 329

Harmanec P., 1998, A&A 335, 173

Hauck B., Mermilliod M., 1980, A&AS 40, 1

Hayes D.S., 1970, in *Ultraviolet Stellar Spectra and Related Groud Based Observations*, IAU Symp. 36, Reidel, Dordrecht, 83

Irwin, A., 1978, Ph.D. thesis, University of Toronto.

Johnson H.L., Mitchell R.I., Iriarte B., Wiśniewski W.Z., 1996, Comm. Lunar Planet. Lab. No. 63, Vol.4, Part 3, 99

Jung J., 1970, A&A 4, 53

Kamp L.W., 1978, ApJS 36, 143

Klinglesmith D.A., 1971, Hydrogen Line Blanketed Model Stellar Atmospheres, NASA SP-3065, Washington, U.S. Government Printing Office

Klochkova V.G., 1985, Pisma AZh 11, 502

Klochkova V.G., 1991, Com. Special Astrophys. Obs. 66, 5

Kroll R., Schneider H., Catalano F.A., Voigt H.H., 1987, A&AS 67, 195

Leone F., 1993, A&A 273, 509

Leone F., Umana G., 1993, A&A 268, 667

Lester J.B., 1972, ApJ 178, 743

Levato A., 1975, A&AS 19, 91

Maitzen H.M., 1981, A&A 95, 213 and priv. com.

McNamara D.H., Larsson H.J., 1962, ApJ 135, 748

Millward C.G., Walker, G.A.H. 1985, ApJS 57, 63

Moon T.T., Dworetsky M.M., 1985, MNRAS 217, 305

Morgan W.W., Lodén K., 1966, Vistas Astron. 8, 83

Morrell N., Levato H., 1991 ApJS 75, 965

Napiwotzki R., Schönberner D., Wenske V., 1993, A&A 268, 653

Odell A.P., 1986, in *Hydrogen Deficient Stars and Related Objects*, Proc. of the IAU Col. 87, Ed. by K. Hunger, D. Schönberner and N. Kameswara Rao, Reidel, Dordrecht, p. 301

Odell A.P., Lebofsky M., 1984, A&A 140, 468

Odell A.P., Voels S.A., 1986, in *Hydrogen Deficient Stars and Related Objects*, Proc. of the IAU Col. 87, Ed. by K. Hunger, D. Schönberner and N. Kameswara Rao, Reidel, Dordrecht, p. 297

Oke J.B., Schild R.E., 1970, ApJ 161, 1015

Pedersen H., Thomsen B., 1977, A&AS 30, 11

Pedersen H., 1979, A&AS 35, 313

Perryman M.A.C., Høg E., Kovalevsky J., Lindegren L., Turon C., 1997, ESA SP-1200, *The Hipparcos and Tycho Catalogues*

Phillips R.B., Lestrade J.-F., 1988, Nat 334, 329

Plaskett J.S., Pearce J.A., 1931, Publ. Dominion Astrophys. Obs. 5, 1

Schild R.E., Chaffee F., 1971, ApJ 169, 529

Shore S.N., Adelman S.J., 1981, in *Upper Main Sequence Chemically Peculiar Stars*, Proc. of the 23rd Liège Astrophys. Col., Liége, Institut d'Astrophysique, 429

Shore S.N., Brown D.N., 1990, ApJ 365, 665

Škoda P., 1996, in Astronomical Data Analysis Software and Systems V, eds. G.H. Jacoby & J. Barnes, A.S.P. Conference Series, Vol. 101, ASP, San Francisco, 187

Stellingwerf R.F., 1978, ApJ 224, 953

Walborn N., 1974, ApJ 191, L95

Walborn N., 1983, ApJ 268, 195

Walker H.J., 1985, A&A 152, 58

Warren W.H., Hesser J.E., 1978, ApJS 36, 497

Wolff S.C., 1990, AJ 100, 1994